ChemComm

COMMUNICATION

View Article Online
View Journal

Cite this: DOI: 10.1039/d5cc03097h

Received 2nd June 2025,
Accepted 14th July 2025

DOI: 10.1039/d5cc03097h

rsc.li/chemcomm

Molecular engineering of benzotriazole-based polymer donors for high performance all-polymer solar cells†

Jiawei Ru,[a] Mengzhen Du,*[b] Jieying Cao,[b] Xin Liu,[b] Hongjun Cheng,[b] Lin Hu,[b] Qing Guo,*[a] Zhihong Xu,[c] Chao Li[a] and Erjun Zhou*[b]

Three BTA-based polymers J52-F, PE3 and PE3-FCl, are utilized to investigate the effects of molecular configuration change and asymmetric halogen substitution on the device performance of all-PSCs. Ultimately, the binary all-PSCs based on PE3-FCl:PY-IT achieve a record power conversion efficiency (PCE) of 17.73%, which is among the highest values for all-PSCs containing BTA-based polymers.

All-polymer solar cells (all-PSCs) have emerged as a promising photovoltaic technology due to their excellent mechanical flexibility, enhanced stability, and compatibility with large-scale fabrication.[1,2] Recently, breakthroughs have significantly advanced the power conversion efficiencies (PCEs) of all-PSC devices, driven by synergistic innovation in novel material design[3] and optimized device fabrication processes.[4,5] For polymer acceptors, the evolution from early materials like N2200 to state-of-the-art systems such as PY-IT[1] has resulted in dramatic performance improvements. For polymer donors, on the one hand, researchers have successfully designed novel molecular structures.[6] On the other hand, most high-efficiency systems still rely on classical acceptor units, such as benzo[1,2-*b*:4,5-*b*′]dithiophene (BDD)[5,7] and dithieno[2,3-*d*:2′,3′-*d*′]benzo[1,2-*b*:4,5-*b*′]dithiophene (DTBT) unit.[8] Both of these strategies collectively promote the all-PSC performance enhancement. Therefore, designing donor polymers with novel A-units or classical A-unit re-engineering strategies is crucial for further enhancing the device efficiency of all-PSCs.

Benzotriazole (BTA) as a classical acceptor unit, renowned for its weak electron-deficient character and the alkyl chain on the N atom being able to modify the crystallinity and solubility of the polymers, has been explored in all-PSCs since as early as 2016.[9] Despite their potential, BTA-based all-PSCs suffer from modest PCEs, primarily attributed to low short-circuit current density (J_{SC}) and fill factor (FF). For instance, in early studies, BTA-based polymer donors with weak crystallinity, when paired with highly crystalline acceptor materials, suffered from inhomogeneous phase-separation domains, resulting in substantial charge recombination within the system.[10] Although the development of novel polymer acceptors has partially mitigated these issues, the inherent limitation of weak crystallinity in BTA-based polymers remains unresolved, which is a key point for improved BTA-based device performance.[11,12]

In this work, we propose a dual-strategy molecular engineering approach to overcome these challenges. Inspired by our previous success in polymer donor/small-molecule acceptor systems – where replacing central thiophene units with fused thieno[3,2-*b*]thiophene (TT) units extended the conjugated backbone, enhanced crystallinity, and boosted charge carrier mobility.[11,13] Herein, we apply such methods to BTA-based all-polymer systems and select J52-F and PE3 with different π-bridges to match with PY-IT in order to verify the generalizability of the method to modulate the morphology of BTA-based active layers. Furthermore, PE3-FCl substitutes one of the fluorine (F) atoms of the BTA unit in PE3 with a chlorine (Cl) atom, to minimize non-radiative energy loss and improve the exciton dissociation driving force. Ultimately, the resulting PE3-FCl-based all-PSCs achieve a remarkable PCE of 17.73% with an FF exceeding 75%, which is the highest performance for BTA-based all-PSCs. The results show that extending π-bridges to enhance crystallinity has a good generalization in BTA-based all-PSC systems. Our findings provide critical insights into molecular design rules for balancing crystallinity and energetic alignment in next-generation all-PSCs.

The structures of J52-F, PE3, PE3-FCl and PY-IT are illustrated in Fig. 1a and b. The number-average molecular weights (M_n) of the three copolymers (J52-F, PE3, PE3-FCl) are 22.5, 22.4 and 28.6 kDa, respectively, and the corresponding polydispersity indices (PDI) are 2.1, 2.7 and 2.8, respectively

[a] School of Materials Science and Engineering, Zhengzhou University, Zhengzhou, 450001, China. E-mail: qingg319@zzu.edu.cn
[b] College of Biological and Chemical Engineering, Jiaxing University, Jiaxing 314001, China. E-mail: dumengzhen@zjxu.edu.cn, zhouej@nanoctr.cn
[c] College of Chemical and Materials Engineering, Xuchang University, Xuchang, Henan 461000, China

† Electronic supplementary information (ESI) available. See DOI: https://doi.org/10.1039/d5cc03097h

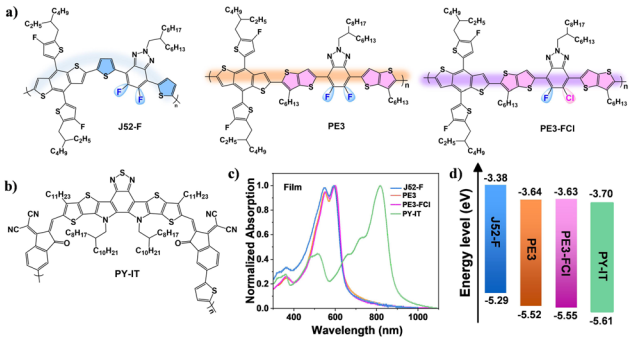

Fig. 1 Chemical structure of (a) J52-F, PE3 and PE3-FCl; (b) PY-IT; (c) UV-vis absorption spectra; (d) energy level diagram of the studied materials.

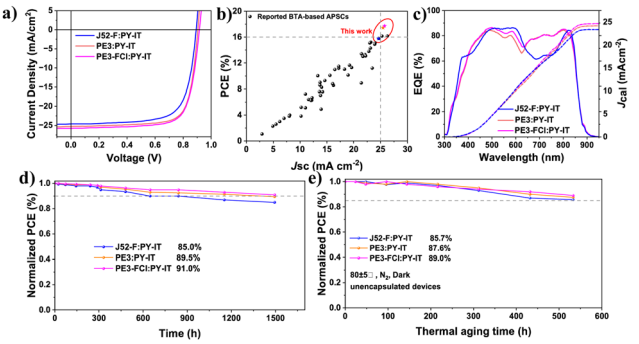

Fig. 2 (a) The J–V curves; (b) the PCE against J_{SC} scatter diagram of the reported BTA-based All-PSCs; (c) EQE spectra; (d) the device stability under a N_2 environment at room temperature; and (e) the device stability under a N_2 environment at a sustained elevated temperature of 80 ± 5 °C.

(Fig. S1–S3, ESI†). The close similarity in both M_n and PDI values across these polymers indicates that the subsequent experimental variations can be primarily attributed to structural differences rather than molecular weight effects. This validates the comparability of the dataset and establishes a controlled basis for interpreting structure–property relationships. Compared to J52-F, the normalized ultraviolet-visible (UV-Vis) absorption spectra of polymers PE3 and PE3-FCl exhibit a distinct red shift, and their shoulder peaks become more pronounced, as presented in Fig. 1c. These observations indicate that the TT-π bridge effectively enhances intermolecular interactions and π–π stacking, thereby benefiting the improvement of J_{SC}. Cyclic voltammetry (CV) measurements were conducted to determine the energy levels of the four polymers. The HOMO and LUMO energy levels are determined as −5.29/−3.38 eV for J52-F, −5.52/−3.64 eV for PE3, −5.55/−3.63 eV for PE3-FCl, and −5.61/−3.70 eV for PY-IT,[12,14] as shown in Fig. 1d. The progressively lowered energy levels of the three donor polymers are beneficial to increasing the V_{OC}.

To systematically evaluate the impact of molecular engineering on device performance, we integrated photovoltaic device fabrication, photophysical characterization, and multi-scale morphological analysis, establishing a comprehensive structure–property relationship chain from molecular structure to macroscopic performance. Devices with the structure ITO/PEDOT:PSS/active layer/PNDIT-F3N/Ag were fabricated. As shown in Fig. 2a, the reference system J52-F:PY-IT exhibited a PCE of 15.78%, with detailed photovoltaic parameters listed in Table 1 and Tables S1–S3 (ESI†). By employing a molecular engineering strategy to introduce a TT unit as the π-bridge, the PE3:PY-IT system achieved a significantly improved PCE of 17.43%, characterized by a V_{OC} of 0.905 V, a J_{SC} of 25.45 mA cm^{-2}, and a FF of 75.71%. Further adopting an asymmetric F/Cl halogen substitution strategy, the PE3-FCl:PY-IT system demonstrated the highest device efficiency of 17.73%, with a V_{OC} of 0.915 V, J_{SC} of 25.76 mA cm^{-2} and FF 75.23%. It is worth noting that this binary device performance is one of the highest PCE values reported to date for BTA-based all PSCs, as shown in Fig. 2b and Table S4 (ESI†). Fig. 2c shows that the integrated current values from the EQE spectra of each system are in excellent agreement with the J–V test results, confirming the

Table 1 Photovoltaic performance of the OSCs based on the three blend films under the illumination of AM 1.5 G, 100 mW cm^{-2}

Active layer	V_{OC} [V]	J_{SC}/(J_{cal})[a] [mA cm^{-2}]	FF [%]	PCE [%] (average)[b]
J52-F:PY-IT	0.892	24.62/(23.39)	71.88	15.78 (15.64 ± 0.14)
PE3:PY-IT	0.905	25.45/(24.17)	75.71	17.43 (17.28 ± 0.15)
PE3-FCl:PY-IT	0.915	25.75/(24.47)	75.23	17.73 (17.67 ± 0.23)

[a] The integral J_{SC} from the EQE curves in brackets. [b] The average values of the device parameters based on 10 devices.

reliability of the measured data. In addition, the long-term stability of the devices is a critical performance indicator in the commercialization process of all-PSCs. Therefore, we systematically evaluated the stability performance of three device systems under nitrogen (N_2) environment storage at room temperature and at a sustained elevated temperature of 80 ± 5 °C. As shown in Fig. 2d, the J52-F-based device had 85% of the original efficiency after 1500 h. The PE3:PY-IT and PE3-FCl:PY-IT devices based on the extended conjugated backbone structure still maintained 89.5% and 91.0% of their initial PCE, which displayed excellent device stability. In addition, thermal stability tests by sustained thermal annealing at 80 ± 5 °C for 500 h showed that the PE3-FCl:PY-IT system maintained 89% of its initial PCE higher than that of the PE3 and J52-F based systems, which were 87% and 85% (Fig. 2e). These results indicate that the linear molecular configuration has a significant modulating effect on the intrinsic stability of the devices.

To better understand the influence of the molecular conformation on photovoltaic performance, the exciton dissociation probabilities $P(E,T)$, charge transfer, carrier mobilities, and charge recombination of the related OSCs were investigated. The $P(E,T)$ can be expressed with $J_{ph}/J_{ph,sat}$, where J_{ph} (photocurrent density) is defined as $J_{ph} = J_L - J_D$ (J_L and J_D represent the current densities under illumination and in dark conditions, respectively). $J_{ph,sat}$ denotes the saturation photocurrent density. The effective voltage (V_{eff}) is obtained according to the formula $V_{eff} = V_0 - V_{appl}$, where V_0 is the voltage at which J_{ph} is

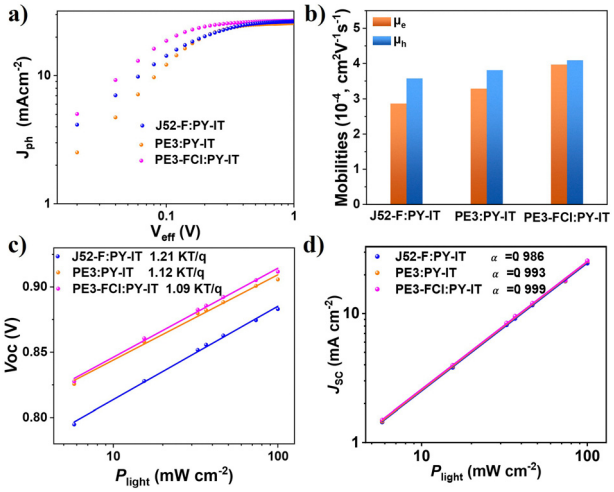

Fig. 3 (a) J_{ph} *vs.* V_{eff}; (b) visual histogram of carrier mobilities; (c) the V_{OC} *versus* light intensity; (d) the J_{SC} *versus* light intensity for the optimized devices.

0, and V_{appl} is the applied external voltage.[15] As estimated from Fig. 3a, the $P(E,T)$ values for the J52-F-, PE3- and PE3-FCl-based devices are 98.6%, 99.3% and 99.9% under short-circuit conditions, and 83.4%, 88.3% and 90.8% under maximum power output conditions, respectively. The highest $P(E,T)$ values of the PE3-FCl-based device indicate excellent exciton dissociation and charge collection efficiencies, which are consistent with the improved J_{SC} and FF of the device.

Then, the carrier mobilities of the blended films measured by space-charge limited current measurement (SCLC) are presented in Fig. S4 and Table S5 (ESI†).[16] The hole and electron mobilities (μ_h and μ_e) of the J52-F-, PE3- and PE3-FCl-based blend films are calculated to be $3.57 \times 10^{-4}/2.87 \times 10^{-4}$, $3.81 \times 10^{-4}/3.29 \times 10^{-4}$, and $4.09 \times 10^{-4}/3.97 \times 10^{-4}$ $cm^2\ V^{-1}\ s^{-1}$, respectively. As shown in Fig. 3b, devices based on PE3 and PE3-FCl, which exhibit linear molecular configurations and stronger π–π stacking interactions, demonstrate higher hole and electron mobilities. This enhanced charge transport capability is a key factor contributing to their high J_{SC} and FF values. In contrast, the zigzagged conformation of J52-F leads to lower carrier mobilities leading to the inferior J_{SC} and FF values among the tested devices.

Furthermore, charge recombination behaviors were investigated by measuring the J_{SC} and V_{OC} values under varying light intensities (P_{light}). The relationship between the V_{OC} and P_{light} is defined as $V_{OC} \propto nkT/q \ln P_{light}$, where k, T, and q represent the Boltzmann constant, the temperature in Kelvin, and the elementary charge, respectively. As presented in Fig. 3c, the n values for the J52-F-, PE3- and PE3-FCl-based devices are 1.21, 1.12, and $1.09kT/q$, respectively. The lowest n value of the PE3-FCl-based device indicates the suppressed monomolecular recombination. The relationship between J_{SC} and P_{light} can be expressed as $J_{SC} \propto P_{light}^{\alpha}$.[17] Here, α is the exponential factor. A value of $\alpha = 1$ indicates that all of the free charges can be extracted before recombination, and $\alpha < 1$ implies the existence of bimolecular recombination. As exhibited in Fig. 3d, compared with the J52-F-based device (α of 0.986), the other devices give $\alpha \approx 1$, indicating the suppressed bimolecular recombination. The weak monomolecular and bimolecular recombination of the PE3-FCl-based devices is consistent with the high J_{SC} and FF.

To investigate the influence of molecular conformation on crystallinity and molecular orientation, we studied the morphology of three blend films using grazing-incidence atomic force microscopy (AFM) and wide-angle X-ray scattering (GIWAXS). The AFM height images and 3D height images are shown in Fig. 4a and Fig. S5 (ESI†). Under optimal conditions, the root mean square roughness (RMS) values of the J52-F-, PE3-, and PE3-FCl-blend films were 1.95, 1.86, and 1.35 nm, respectively. Compared to other active layers, the J52-F-based device exhibited the highest RMS value, and its 3D height image revealed an inhomogeneous morphology, suggesting the presence of excessive aggregated domains. This is likely due to the lower crystallinity of the non-linear structure, leading to entanglement.[18] Such an inhomogeneous structure may hinder charge collection. Meanwhile, the PE3-FCl-based device showed the smallest RMS value and a smooth surface, and this favorable morphology provides more D/A contact interfaces, facilitating exciton dissociation, which is consistent with the aforementioned improvements in J_{SC} and FF.

The influence of the different molecular conformation and halogen atom substitution on the molecular stacking in the blend films was further investigated through GIWAXS measurements. The recorded lamellar (100) and π–π stacking (010) diffraction peaks, along with the calculated crystalline coherence length (CCL) values, are summarized in Table S6 (ESI†). As shown in the two-dimensional GIWAXS patterns (Fig. 4b and c), three blend films exhibit distinct (010) π–π stacking peaks in the out-of-plane (OOP) direction and prominent (100) lamellar peaks in the in-plane (IP) direction. The high diffraction intensities confirm a face-on molecular orientation, which is

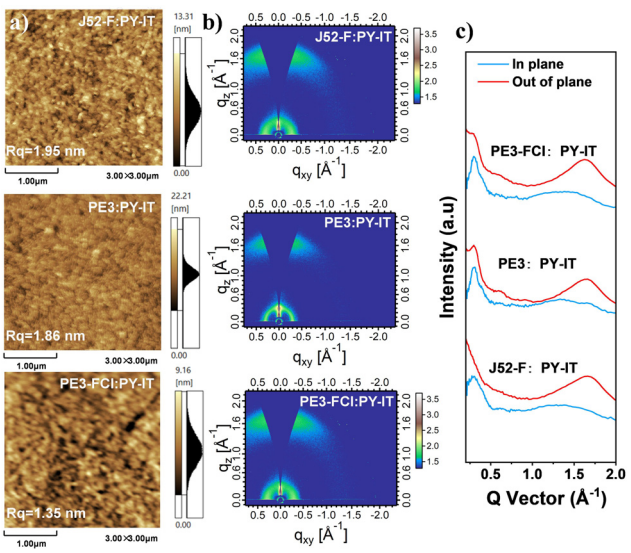

Fig. 4 (a) AFM height images; (b) 2D-GIWAXS patterns of the blended films and (c) the corresponding 1D line-cuts in the in-plane and out-of-plane directions.

beneficial for vertical charge transport. By comparing the CCL values in the IP and OOP directions, it is observed that for the (010) OOP direction peaks, the CCL increases from 20.01 Å for J52-F to 21.66 Å for PE3, which is achieved by modification of the molecular backbone. For the (100) IP direction peaks, the CCL increases dramatically from 36.08 Å for J52-F to 86.74 Å for PE3, suggesting that the linear-structured molecules exhibit superior crystallinity and smoother surfaces, thereby enhancing charge transport. Furthermore, asymmetric substitution of F atoms in PE3 with Cl atoms (forming PE3-FCl) reduces the π–π stacking distances in both the IP and OOP directions while increasing CCL. These results demonstrate that asymmetric halogenation induces more ordered molecular stacking in the PE3-FCl blend films, which facilitates their charge transport and thus improves J_{SC} and FF.

In conclusion, this work systematically investigates the impact of BTA-based polymers with different π-bridges and asymmetric halogen substitutions on the photovoltaic performance of all-PSCs. The results show that the linear-configuration polymers PE3 and PE3-FCl, with TT units as π-bridges, demonstrate enhanced conjugation and optimized active-layer morphology, leading to superior PCE and stability. The polymer PE3-FCl containing an asymmetric halogenation on the BTA unit further deepens the energy levels, and enhances the device's exciton dissociation probability and charge transport properties, thereby again improving the device performance. Remarkably, PE3-based devices achieve a high PCE of 17.43%, and the PE3-FCl-based devices attain a champion PCE of 17.73%, both significantly surpassing the 15.78% efficiency of the reference J52-F-based device. This study establishes the highest reported efficiency for BTA-based all-PSCs, validating the universal applicability of linear backbone engineering and asymmetric halogen substitution strategies of BTA-based polymers. These findings provide critical insights for advancing high-performance and operationally stable BTA-based polymer systems.

The authors are thankful for the support from the National Natural Science Foundation of China (52303259, 52373176).

Conflicts of interest

There are no conflicts to declare.

Data availability

The data supporting this article have been included as part of the ESI.†

Notes and references

1 S. Li, K. Zhou, B. Sun, W. Zhao and L. Ye, *Mater. Today Energy*, 2022, **30**, 101166.
2 K. Zhou, K. Xian and L. Ye, *InfoMat*, 2022, **4**, e12270.
3 (*a*) Q. Bai, Q. Liang, Q. Liu, B. Liu, X. Guo, L. Niu and H. Sun, *Chin. J. Chem.*, 2023, **41**, 3714–3728; (*b*) Z. Ge, J. Qiao, Y. Li, J. Song, C. Zhang, Z. Fu, M. H. Jee, X. Hao, H. Y. Woo and Y. Sun, *Adv. Mater.*, 2023, **35**, 2301906; (*c*) J. Song, C. Li, H. Ma, B. Han, Q. Wang, X. Wang, D. Wei, L. Bu, R. Yang and H. Yan, *Adv. Mater.*, 2024, **36**, 2406922; (*d*) X. Zhang, H. Gao, Y. Kan, X. Wang, W. Zhang, K. Zhou, H. Xu, L. Ye, R. Yang and Y. Yang, *Angew. Chem., Int. Ed.*, 2025, **137**, e202415583.
4 (*a*) H. Ma, J. Song, J. Qiao, B. Han, Q. Wang, M. H. Jee, L. Bu, D. Wei, H. Y. Woo and X. Hao, *Energy Environ. Sci.*, 2025, **18**, 397–405; (*b*) X. Wu, B. Xiao, R. Sun, X. Yang, M. Zhang, Y. Gao, B. Xiao, E. D. Papkovskaya, Y. Luponosov and C. J. Brabec, *Energy Environ. Sci.*, 2025, **18**, 1812–1823; (*c*) J. Zhu, R. Zeng, E. Zhou, C. Li, J. Deng, M. Du, Q. Guo, M. Ji, Z. Wang, Y. Lin, F. Han, J. Zhuang, S. Tan, L. Kan, L. Zhu, M. Zhang and F. Liu, *J. Am. Chem. Soc.*, 2025, **147**, 24491–24501.
5 R. Zeng, L. Zhu, M. Zhang, W. Zhong, G. Zhou, J. Zhuang, T. Hao, Z. Zhou, L. Zhou and N. Hartmann, *Nat. Commun.*, 2023, **14**, 4148.
6 (*a*) Z. Hu, J. Wang, C. Cui, T. Liu, Y. Li, L. Song, S. Wen and X. Bao, *Small*, 2024, **20**, 2311648; (*b*) J. Wang, Y. Cui, Y. Xu, K. Xian, P. Bi, Z. Chen, K. Zhou, L. Ma, T. Zhang and Y. Yang, *Adv. Mater.*, 2022, **34**, 2205009; (*c*) Z. Wang, X. Wang, L. Tu, H. Wang, M. Du, T. Dai, Q. Guo, Y. Shi and E. Zhou, *Angew. Chem., Int. Ed.*, 2024, **136**, e202319755; (*d*) J. Zhang, Q. Huang, K. Zhang, T. Jia, J. Jing, Y. Chen, Y. Li, Y. Chen, X. Lu and H. Wu, *Energy Environ. Sci.*, 2022, **15**, 4561–4571; (*e*) S. Zhang, M. Cai, C. Shang, F. Bi, F. Feng, Z. Du, C. Sun, Y. Li and X. Bao, *Adv. Funct. Mater.*, 2023, **33**, 2301701.
7 (*a*) Q. Liang, H. Li, W. Xu, J. Lu, R. Ma, Q. Bai, X. Sun, M. Chen, L. Zhu and Q. Liu, *Angew. Chem., Int. Ed.*, 2025, **64**, e202425267; (*b*) W. Qiu, C. Liao, Y. Li, M. Deng, Y. Duan, X. Xu and Q. Peng, *Adv. Funct. Mater.*, 2025, 2503009; (*c*) J. Wang, C. Sun, Y. Li, F. Bi, H. Jiang, C. Yang, X. Bao and J. Chu, *Nat. Commun.*, 2025, **16**, 1784.
8 (*a*) J. Wang, Y. Wang, K. Xian, J. Qiao, Z. Chen, P. Bi, T. Zhang, Z. Zheng, X. Hao and L. Ye, *Adv. Mater.*, 2024, **36**, 2305424; (*b*) Y. Wu, P. Li, S. Yu, Y. Min and L. Xiao, *Molecules*, 2024, **29**, 2879.
9 L. Gao, Z.-G. Zhang, L. Xue, J. Min, J. Zhang, Z. Wei and Y. Li, *Adv. Mater.*, 2015, **28**, 1884–1890.
10 (*a*) Z. Li, R. Xie, W. Zhong, B. Fan, J. Ali, L. Ying, F. Liu, N. Li, F. Huang and Y. Cao, *Solar RRL*, 2018, **2**, 1800196; (*b*) Q. Zhang, Z. Chen, W. Ma, Z. Xie and Y. Han, *J. Mater. Chem. C*, 2019, **7**, 12560–12571.
11 M. Du, A. Tang, J. Yu, Y. Geng, Z. Wang, Q. Guo, Y. Zhong, S. Lu and E. Zhou, *Adv. Energy Mater.*, 2023, **13**, 2302429.
12 M. Du, J. Yu, H. Jiang, Z. Song, Y. Geng and E. Zhou, *ACS Macro Lett.*, 2024, **13**, 1240–1244.
13 (*a*) Y. Chen, Y. Geng, A. Tang, X. Wang, Y. Sun and E. Zhou, *Chem. Commun.*, 2019, **55**, 6708–6710; (*b*) Y. Chen, P. Lei, Y. Geng, T. Meng, X. Li, Q. Zeng, Q. Guo, A. Tang, Y. Zhong and E. Zhou, *Sci. China Chem.*, 2023, **66**, 1190–1200; (*c*) J. Zhou, P. Lei, Y. Geng, Z. He, X. Li, Q. Zeng, A. Tang and E. Zhou, *J. Mater. Chem. A*, 2022, **10**, 9869–9877.
14 A. Tang, B. Xiao, F. Chen, J. Zhang, Z. Wei and E. Zhou, *Adv. Energy Mater.*, 2018, **8**, 1801582.
15 (*a*) P. W. Blom, V. D. Mihailetchi, L. J. A. Koster and D. E. Markov, *Adv. Mater.*, 2007, **19**, 1551–1566; (*b*) L. Lu, W. Chen, T. Xu and L. Yu, *Nat. Commun.*, 2015, **6**, 7327.
16 P. Murgatroyd, *J. Phys. D. Appl. Phys.*, 1970, **3**, 151.
17 S. R. Cowan, A. Roy and A. J. Heeger, *J. Phys. D: Appl. Phys.*, 2010, **82**, 245207.
18 C. Li, J. Zhou, J. Song, J. Xu, H. Zhang, X. Zhang, J. Guo, L. Zhu, D. Wei and G. Han, *Nat. Energy*, 2021, **6**, 605–613.

